Review

Israel Journal of Chemistry

doi.org/10.1002/ijch.202100076

Emerging Trends in Chiral Inorganic Nanostructures

Jun Lu[+],[a, b] Yao Xue[+],[c] and Nicholas A. Kotov*[a, b, d]

Abstract: The transfer of structural mirror asymmetry from chiral molecules to the inorganic phase at solid-liquid interfaces enabled rapid development of biomimetic chiral nanoparticles. They can be synthesized and assembled following a variety of chemical methods resulting in the broad family of chiral inorganic nanostructures (CNs). Their chemistry attracted large attention due to marked enhancement of circular dichroism and polarization rotation compared to organic molecules and particles, which opened application prospects in sensing, imaging, catalysis, nonlinear optics, electronics, and medicine. New physical, chemical and biological effects involving CNs such as giant optical activity, mechanical force-assisted modulation of optical activity, photon-to-particle chirality transfer and suppression of amyloid toxicity have been observed. Marked strides toward enhancement of optical asymmetry (*g*-factor), engineering dynamic chirality in nanostructures, and spectral range of optical activity of chiral inorganic nanostructures from the ultraviolet to terahertz regions have also been made. Here, we summarize these and other current trends in the research of chiral inorganic nanomaterials and offer our perspective how the fundamental and translational research in this area is likely to develop in the next two decades.

Keywords: chirality · chiral inorganic nanostructures · *g*-factor · circular dichroism · dynamic modulation

Chirality is a geometric property describing objects with non-superimposable mirror images. Most of the molecules in nature and living organisms are chiral, leading to the great importance of this geometrical property in pharmacy, biotechnology, and catalysis. Chirality research spans multiple disciplines, for example, chemistry, materials, mathematics, physics, and biology and has attracted widespread attention. Prior studies[1] about the transfer of mirror asymmetry from organic molecules to inorganic phase established in macrocrystals[2–4] and Langmuir-Blodgett monolayers[5] paved the way for the rapid development of chiral biomimetic nanomaterials, which has gradually become one of the most dynamic areas of nanomaterial research. In addition to the significance of the questions of the origin of life[3,6–9] amplified by the universal ability of nanoparticles (NPs) to self-assemble into complex structures[10,11] and transfer mirror asymmetry from photons to matter,[12,13] the interest in chiral nanostructures (CNs) is driven by pragmatic matters. Due to fundamental physical properties and scale of inorganic materials,[14,15] CNs that include chiral NPs, nanorods (NRs), nanohelices, superstructures and others, reveal exceptionally large circular dichroism (CD), optical rotation dispersion (ORD) and, more recently, *g*-factors. Such light-matter interactions are sometimes referred to as giant optical activity[16–18] or superchirality.[19,20] From the initial observation to individual metal and semiconductor NPs,[21,22] it was revealed that optical activity can be dramatically enhanced by assembling NPs into superstructures at higher scale.[23,24] The large optical activity of CNs is associated with their multiscale chirality, highly polarizable components, and plasmonic effects.[14,24–30] The enhancement of asymmetric light-matter interactions also encompasses circular polarized light emission,[11,31] nonlinear optics,[32] charge transport,[33] and optoelectronics,[34] all of which bring a range of new applications in sensing,[35] display,[14] catalysis,[36] optical devices,[27] nanorobotics,[37] spintronics,[38] etc.

Several electronic effects can give rise to the optical asymmetry of CNs (Figure 1). *First*, the chiroptical activity originates from the asymmetry of atoms and atomic orbitals at the interface of inorganic core with chiral organic ligands,[39–41] which is quite similar to the origin of CD peaks observed for typical organic molecules. This type of optical activity is observed for nearly all CNs.

Second, the long- and short-range coupling of electron wave functions of molecules and inorganic cores creates chiroplasmonic optical activity that is typically associated with metal NPs.[23,42,43] Inclusion of both electrostatic and magnetic dipoles is essential for understanding the coupling mechanisms in the cases of metallic and other highly polarizable NPs.[44] Typical examples of (bio)organic molecules, whose chirality can be transferred to CNs,[43,45] include DNA,[45] amino acids,[46] and peptides.[47]

[a] *J. Lu,[+] N. A. Kotov*
Department of Chemical Engineering, University of Michigan, Ann Arbor, MI 48109, USA
E-mail: kotov@umich.edu
[b] *J. Lu,[+] N. A. Kotov*
Biointerfaces Institute, University of Michigan, Ann Arbor, MI 48109, USA
[c] *Y. Xue[+]*
State Key Laboratory of Supramolecular Structure and Materials, College of Chemistry, Jilin University, Changchun, China
[d] *N. A. Kotov*
Department of Materials Science, University of Michigan, Ann Arbor, Michigan 48109, United States
[+] *These authors contributed equally to this work.*

Third, strong chiroptical activity can be found in chiral NPs with intrinsic chiral lattice groups such as the case of $P2_12_12_1$, $P3_121$, and $P3_221$.[48] However, NPs with these chiral space groups are limited in nature, mainly composed of Se,[49] Te,[50] terbium orthophosphate monohydrate ($TbPO_4 \cdot H_2O$),[51] and α-HgS[52].

Fourth, chiral ligands adsorbed on the surface of NPs can also lead to chirality distorted crystal lattices and enhanced appearance of twist dislocations in the inorganic core.[36,44,53–55] Such effects have been observed for semiconductor[11,53,54] and ceramic[36,44] NPs, small metal clusters,[56,57] and nanocarbons.[41] Recently, similar effects were observed for lead-iodide perovskites.[58] To observe such effects, chiral molecules with strong binding to NP surfaces, typically with at least two attachment points to the NPs *via* coordination or covalent bonds are needed.

Fifth, achiral or racemic NPs asymmetrically arranged in 3D space can generate strong enhancement of CD and *g*-factor spectra during the self-assembly process.[23,59,60] This effect is typically observed for metal NPs because of strong long-range coupling of plasmonic states[61] although it may also involve the coupling between plasmons and excitons.[62–66] Chiral templates such as DNA,[62,67] peptides,[68,69] cellulose nanocrystals,[70] liquid crystals,[71] supramolecular fibers,[24] and polymers[72] have been used for the self-assembly of semiconductor[73,74] and plasmonic NPs.[67,68]

Sixth, markedly enhanced polarization rotation was also found in 2D chiral patterns with 3D components imparted by top-down synthesis methods, including focused ion beam-induced deposition,[75] laser writing,[27] glancing-angle deposition,[76] electron beam lithography,[77] and kirigami cuts.[78,79]

Starting with fairly simplistic geometric, electronic, and optical arguments,[21,25,80] the understanding of the origin and details of exceptionally strong optical activity has reached unprecedented depth due to extensive effort invested in CN fabrication and modeling. Numerous chirality-related properties, such as external field sensitive circular dichroism and circularly polarized emission,[44] second harmonic generation,[32] and ferroelectrics,[81] as well as new chiral-related applications, for example, biomimetic chiral catalysis,[36,82] 3D display,[14] and spin electronic devices[38] are being quickly developed. However, for practical needs, the *g*-factors for the majority of CNs still need to be improved. Another limitation is that most of these chiral assemblies are static. While real-time reconfigurable CNs are beginning to emerge,[44,78,83–85] big strides in this direction are still needed for the realization of sensors, catalysts, displays, and other photonic devices. In this minireview, we summarize current and emerging trends of CNs, including the development of chiral NPs and nanostructures with high *g*-factors, modulation of chiroptical activities, and related applications.

From High CD Amplitude to High *g*-Factor

Optical asymmetry *g*-factor, that is, the ratio of the difference to the sum of extinction under left- and right-handed circularly polarized light (LCP/RCP), is an important parameter for CNs that enumerates their chiroptical activities. Engineering NPs and nanostructures with high *g*-factors are highly desired for the realization of a wide range of chiral-related applications such as sensing, display, catalysis, circular polarized sources, electronic and optical devices. The following discussion offers specific approaches for optimizing *g*-factors for various CNs.

Molecule dipole resonance. The *g*-factors of NPs with chirality stemming from the electronic dipole-dipole interaction of chiral molecules on NPs are normally small. For

Jun Lu finished his PhD studies from Prof. Kun Liu's group in the Department of Chemistry, Jilin University, Changchun in 2017. He is now a postdoc research fellow in Prof. Nicholas A. Kotov's group in the Department of Chemical Engineering, University of Michigan in Ann Arbor, MI. His research focus on the understanding of chemical and physical insight behind the self-assembly of inorganic NPs, magnetism and chiromagnetic properties of semiconductor NPs and assemblies, and exploring the potential applications for CNs.

Yao Xue received her B.S. degree in Chemistry from Jilin University, China in 2017. Currently, she is a PhD candidate supervised by Prof. Kun Liu's group in the Department of Chemistry, Jilin University. Her research focus on the self-assembly of inorganic nanoparticles, detection of polymer conformation by NMR and the effect of polymer conformation on the organ accumulation of nanomedicine.

Nicholas A. Kotov obtained his PhD in chemistry from Moscow State University in 1990. He is currently the Irving Langmuir Distinguished Professor of Chemical Sciences and Engineering of the University of Michigan in Ann Arbor, MI. His research interests encompass self-assembly of inorganic NPs, chirality of NPs and selected biosensing effects of plasmonic nanomaterials and biomimetic inorganic nanostructures and applications in optics, batteries and catalysis.

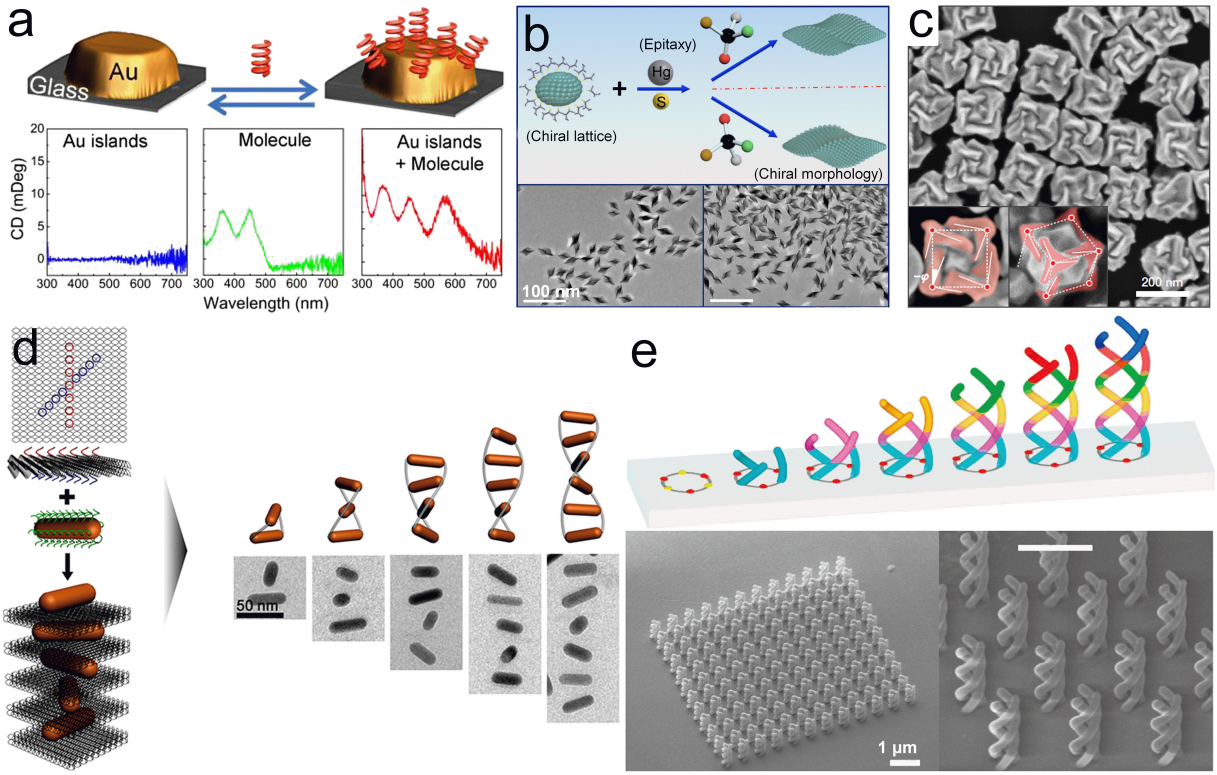

Figure 1. Strategies for inorganic nanostructures to obtain chiroptical activity. (a) Adsorption of helical riboflavin on achiral gold islands on glass substrates. Reproduced with permission from ref. [43]. Copyright 2013 American Chemical Society. (b) Helical α-HgS NPs epitaxially regrown on twisted seeds with chiral lattices. Reproduced with permission from ref. [52]. Copyright 2017 Springer Nature. (c) TEM image of gold helicoid NPs without chiral lattices but with distorted surfaces. Reproduced with permission from ref. [14]. Copyright 2018 Springer Nature. (d) DNA origami fabricated helical nanostructures with achiral gold NRs. Reproduced with permission from ref. [67]. Copyright 2015 American Chemical Society. (e) Triple-helical nanowire arrays engineered by an innovative tomographic rotatory growth method combined with focused ion beam-induced deposition. Reproduced with permission from ref. [75]. Copyright 2015 Springer Nature.

example, for the cysteine-capped semiconductor NPs, such as CdSe[46] and CdTe,[86] the magnitude of *g*-factors are around 2.0×10^{-4} (Table 1), which is even weaker than those of most chiral molecules, for example, DNA[87] and peptides.[88] Optimization of the chemical binding of chiral molecules on NP surface[89] can lead to their well-oriented, self-assembled monolayer, which is critical to the enhancement of coupling effect between chiral molecules and NPs.[90] Controlling the orientation of NPs[43] and increasing the local electric field intensity[91] also increases the optical asymmetry. However, the use of these chemical approaches has had limited success in enhancing *g*-factors, with magnitudes remaining below 1.0×10^{-3}.

Chiral crystal lattices. The *g*-factors of NPs made from materials possessing chiral crystal lattices are in the range of 1.0×10^{-3} to 2.0×10^{-2} (Table 1), which are almost ten times larger than the *g*-factors obtained from chiral molecule dipole coupling with NPs. The higher *g*-factors should be primarily attributed to the chiral shapes of NPs that increase the scale of chirality and thus reduce the dimensional mismatch between the chiral features and the light wavelength. In the work of Markovich and co-workers on Te nanocrystals,[50] NPs with twisted shapes showed higher CD signals than NPs with achiral morphologies, but in the work of Ouyang and co-workers on α-HgS colloids,[52] NPs with helically twisted morphologies presented identical *g*-factors compared to NPs with achiral shapes, such as nanocubes, nanorods, and nanowires (Figure 1b). This indicates the relevance of additional factors exemplified by the electric properties of the materials in different crystal forms. The size of NPs also plays an important role. Te NPs[50] with larger sizes exhibited stronger *g*-factors, while the in case of smaller α-HgS,[52] the trend was opposite.

Particle shapes. Uniquely high *g*-factors were obtained when NP surfaces were optimized into chiroplasmonic NPs with unique shapes that displayed nanoscale chirality and polydispersity of the chiral metallic centers. Nam and co-workers,[14] showed that three-dimensional gold helicoids with intricate high-Miller-index facets (Figure 1c) generated high *g*-factors of 2.0×10^{-1}. An even higher *g*-factor was reported by Liz-Marzán and co-workers,[92] who synthesized chiral wrinkle covered nanorods with chiral micelles as covering ligands with a *g*-factor that reached to 0.28, which is larger than any chiral materials measured in random dispersions.

Self-Assembled NP superstructures. Optical activity with high asymmetry can be achieved by organizing NPs in 3D space with specific chiral geometries. This method leads to nanoscale assemblies with *g*-factors in the range of 1.0×10^{-3} to 1.0×10^{-1} (Table 1), which are much larger than those of most single NPs. Another advantage of this technique is that the self-assembly is a universal method; it is not limited to any specific type of NPs, for example, metal, semiconductor, ceramic, isotropic, anisotropic, chiral and achiral NPs, and massive chiral templates can be used such as DNA (Figure 1d), peptides, liquid crystals, polymers, supramolecular assembles, cellulose crystals, etc. A large number of chiral assemblies have been fabricated *via* self-assembly during the last decade. Among them are nanostructures in homogenous and dispersion states with *g*-factors that reached to 0.12,[15] which were observed in a long-range ordered and helically-packed gold NRs chains (Figure 2). The latter were fabricated by Liu, Kotov and co-workers using a co-assembly of human islet amyloid polypeptide (hIAPP) with gold NRs. Compared with individual NRs covered with peptides, these high *g*-factors were enhanced by thousands of times because of the large spectral shift under circularly polarized photons and reduced scattering of energy states with dipoles orientated in an anti-parallel fashion. The NR-hIAPP assemblies presented liquid crystal-like color variations under cross-polarized conditions, which were employed for drug screening for amyloid diseases. Even higher *g*-factors were observed for twisted films on the substrate, for example, crossed gold nanowire layer with controlled inter-layer angles,[93] cross-stacked gold NP chain arrays,[19] and twisted semiconductor layers.[94] However, care needs to be applied when investigating thin solid films with high optical asymmetry.[95] The very high *g*-factors may potentially originate from the orientation-induced linear dichroism or birefringence rather than circular dichroism, which makes it hard to directly compare them with the cases in the dispersion state.

Three points need to be considered when aiming to increase the *g*-factors of assembled CNs: (1) Anisotropic NPs such as gold nanorods (NRs) are better building blocks for self-assemblies compared to isotropic nanoparticles such as gold nanospheres. The *g*-factors of CNs from anisotropic NP assemblies are much higher than those of isotropic NP assemblies. This is because the symmetry breaking for anisotropy NPs is much more easily manifested and aniso-

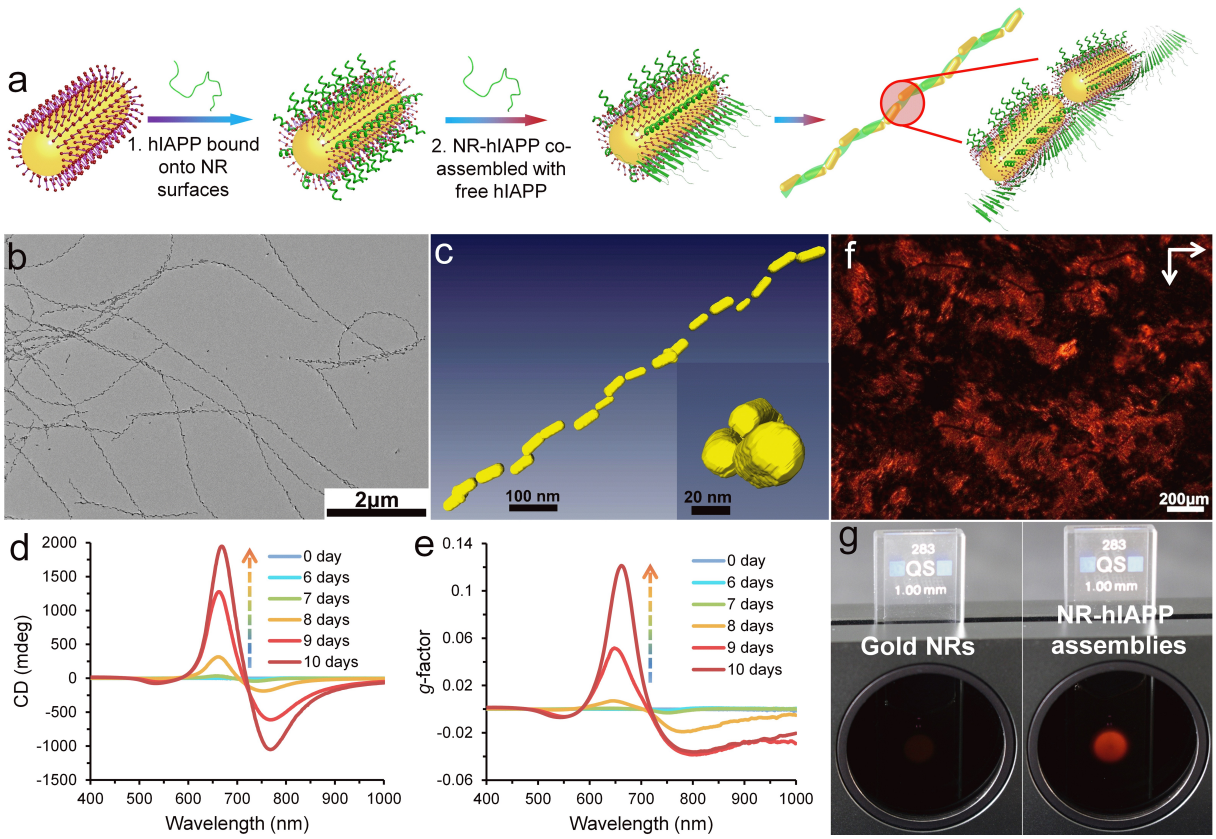

Figure 2. Enhanced *g*-factor *via* the long-range registry of gold NRs. (a) Illustration for the co-assembly process of human islet amyloid polypeptide (hIAPP) with NRs. (b, c) TEM (b) and reconstructed cryo-TEM tomography images (c) of the co-assembled helices. (d, e) CD (d) and *g*-factor (e) spectra collected at different times during the co-assembly process. (f) Polarized optical microscopy (POM) image of the helices. (g) Photographs of pure NR and NR-hIAPP assemblies monitored by a digital camera. Reproduced with permission from ref. [15]. Copyright 2021 American Academy for the Advancement of Science.

tropic NPs have stronger resonance models and higher absorption coefficients than their isotropic counterparts; (2) Chiral templates with similar or larger sizes than NPs have a better capacity to arrange NPs for high *g*-factors. With templates such as DNA origami scaffolds, peptide fibers, cellulose nanocrystals, and liquid crystals, the assembled nanostructures generally have complete left- or right-handedness, compared to the enantiomeric excess in a mixture resulting from the use of small chiral molecule templates, for example, amino acids, short peptides, and polymers; (3) Optimized geometrical parameters, such as pitch, length, width, thickness, angle, and interparticle distance of CNs are critical to the generated *g*-factors as these parameters will directly adjust the light-mater interaction process under LCP and RCP illumination.

Fabricated chiral nanostructures. The *g*-factors of CNs fabricated by top-down methods can be as high as 2.6×10^{-1} for platinum nanohelical arrays,[96] 3.0×10^{-1} for planar helical Au heptamer arrays,[97] and 3.7×10^{-1} for triple-helical platinum nanowire arrays (Figure 1e).[75] This is mainly because these arrays have only one perpendicular orientation on the substrate that can generate the maximum absorption cross-section in the light-matter interaction process in comparison to other orientations, while reducing the contribution from scattering. Materials constrains for CNs fabricated by top-down methods need to be noted. Chemistry of the lithographic process restricts the materials choice to only a few metals: Au, Cu, Pd, Pt and Ag. Another disadvantage is that it is difficult to control the nanoscale precision of CNs, which is important for some applications in spintronics, catalysis, and sensing, where mirror asymmetry and specific narrow gaps between the CNs are essential.

Chiroptical Activity with Real-Time Modulation

Dynamic manipulation of the optical activity of CNs provides opportunities to turn on/off and gradually vary chiroptical activity, thus creating a wide range of possibilities in sensing, spintronics, photonics, displays, and catalysis. Two strategies have been used for real-time modulation of chiroptical activity primarily focusing on variation of CD spectra. The most common approach involves the use of environmental conditions such as temperature,[102] pH[84], and light[60] to change the structure of CNs. Some specially selected small molecules can modulate the conformation of the chiral assemblies as well.[103,104] Another approach to modulate optical polarization is based on the mechanical response under external strain to manipulate the geometry[95] and inter-component interactions[19] of chiral superstructures.

Temperature- and media-dependent self-assembly. An early chemical strategy involved the use of different temperature and media conditions to assemble and disassemble CNs to manipulate their chiroptical activities. For example, Kotov, Xu and coworkers observed a distinct change in dihedral angle and distance between side-by-side gold nanorod assemblies

Table 1. Comparison of *g*-factors for various CNs.

Chirality origin	Composition	λ (nm)	*g*-factor	Ref.
Chiral molecules	DNA	300	3.8×10^{-3}	[87]
	Bovine serum albumin	230	6.0×10^{-3}	[88]
	Small molecule assembled helical ribbon	650	6.0×10^{-2}	[98]
Chiral molecule dipole coupling on achiral NPs	Peptide functionalized gold NPs	520	2.2×10^{-4}	[47]
	Cysteine capped CdSe QDs	530	2.3×10^{-4}	[46]
	Chiral supramolecular assemblies on Ag NPs	410	2.5×10^{-4}	[90]
	Riboflavin capped gold islands on substrate	570	7.6×10^{-4}	[43]
Chiral lattices on NPs	Te NPs	350	3.0×10^{-3}	[50]
	α-HgS nanostructures	540	1.4×10^{-2}	[52]
Chiral ligand induced surface distortions	$WO_{3-x}\cdot H_2O$ NPs	560	1.8×10^{-3}	[36]
	Chiral perovskites	660	6.0×10^{-3}	[58]
	Co_3O_4 NPs	550	2.0×10^{-2}	[44]
	Au helicoid NPs	620	2.0×10^{-1}	[14]
	Chiral Au NRs	1450	2.8×10^{-1}	[92]
Chiral molecule induced self-assemblies	DNA assembled NP-QD pyramids	510	8.1×10^{-3}	[62]
	Solvent driven chiral Au cluster assembly	450	8.2×10^{-3}	[99]
	Peptide assembled Au NP helices	670	1.8×10^{-2}	[69]
	DNA origami assembled Au NR helices	800	2.0×10^{-2}	[67]
	Supermolecular fiber as template for Au NRs	750	2.2×10^{-2}	[24]
	Cysteine assembled CdTe helices	1100	6.0×10^{-2}	[73]
	Cysteine assembled Au NR oligomers	580	6.5×10^{-2}	[100]
	hIAPP co-assembled Au helices	660	1.2×10^{-1}	[15]
Chiral morphology through top-down methods	Chiral plasmonic oligomer arrays	1100	1.4×10^{-1}	[101]
	Single platinum nanohelices arrays	600	2.6×10^{-1}	[96]
	Planar helical Au heptamer	850	3.0×10^{-1}	[97]
	Triple-helical platinum nanowire arrays	700	3.7×10^{-1}	[75]

linked together by DNA molecules, achiral sodium carbonate or sodium citrate (Figure 3a).[83] Changes in the electrolyte content of the media can be directly translated to the amplitude of CD peaks. Such process can also be exploited in the dynamic reconfiguration of nanorod dimers when they enter the cellular cytoplasm from the interstitial fluid outside of the cells.[105]

The work of Tang and co-workers[106] reported that gold NRs capped by double-stranded DNA assembled at 20 °C and disassembled at 60 °C, thus generating temperature-dependent chiroplasmonic resonances. However, the related CD peaks had a narrow dynamic range of 0–3 mdeg, which led to a low signal/noise ratio. Larger dynamic range was achieved by Liu and co-workers[102] who used DNA origami to fabricate chiral gold NR dimers with thermal re-configurability (Figure 3c). At low temperatures, the dimer-based CNs were locked by split adenosine triphosphate aptamers; as the temperature increased, the lock opened and resulted in a relaxed state of NR dimers.

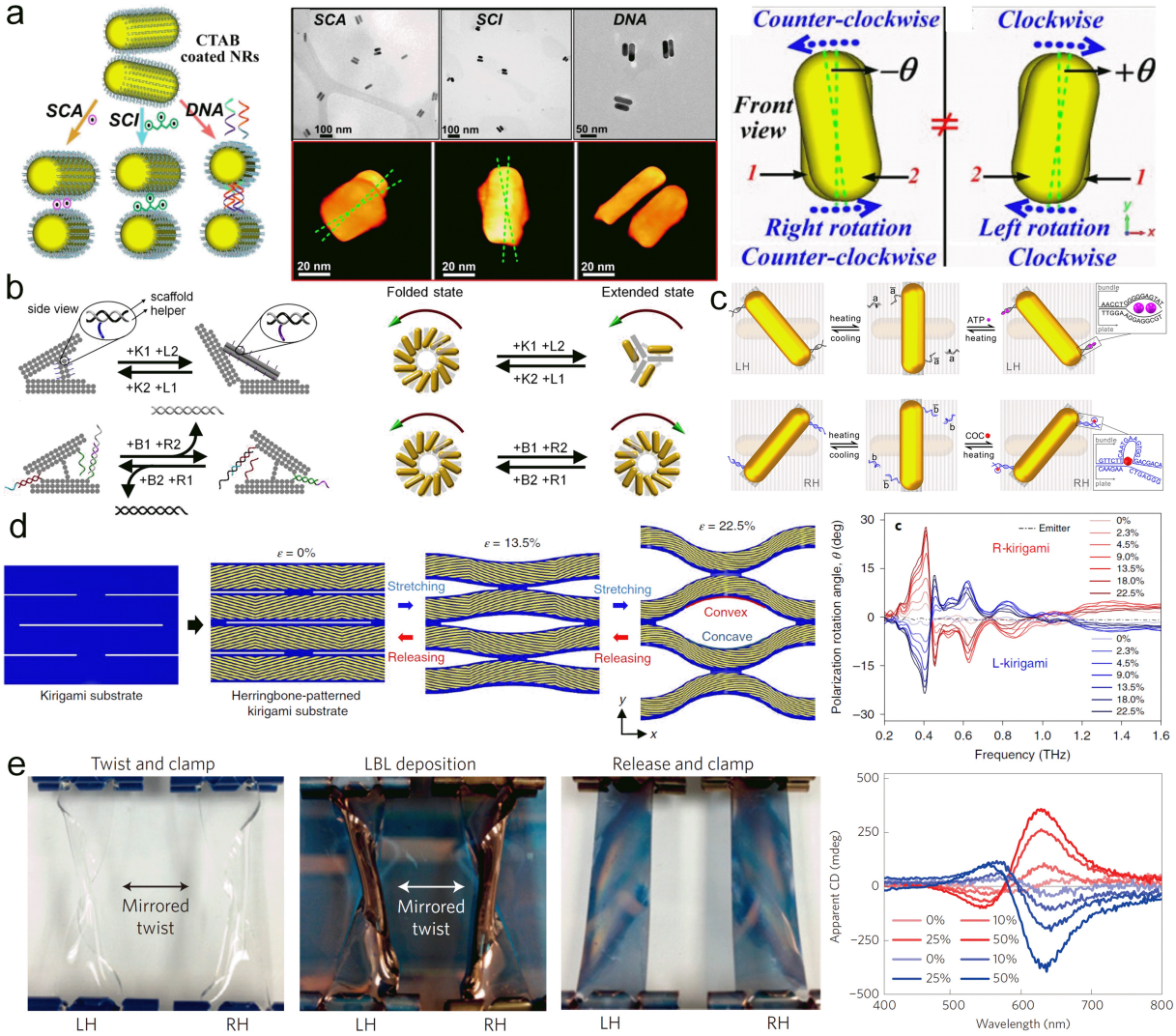

Figure 3. Real-time modulation of chiroptical activities. (a) Gold nanorod dimer with reserved conformation fabricated *via* the self-assembly with sodium citrate (SCI), sodium carbonate (SCA) and DNA. Reproduced with permission from ref. [83]. Copyright 2013 Springer Nature. (b) Reversible process of Au NR helices between folded and extended states and two mirror-image like structures under the integration of DNA origami with displaced DNA strands such as Key and Lock strands [(K1 and L2) or (K2 and L1)] and Block and Release strands [(B1 and R2) or (B2 and R1)]. Reproduced with permission from ref. [103]. Copyright 2018 American Chemical Society. (c) Switchable process of DNA origami fabricated Au NR dimers under the thermal tunability and split adenosine triphosphate (ATP) and cocaine (COC) aptamer-target regulation. Reproduced with permission from ref. [102]. Copyright 2018 American Chemical Society. (d) Kirigami architecture used for the fabrication of herringbone-structured Au strips with terahertz circular dichroism responses under different stretching and releasing intensities. Reproduced with permission from ref. [108]. Copyright 2019 Springer Nature. (e) Strain-modulated rotatory optical activity in gold NP nanocomposites layer-by-layered on Elastic poly(dimethylsiloxane) (PDMS) substrates. Reproduced with permission from ref. [95]. Copyright 2016 Springer Nature.

During the transition between locked and relaxed states, the angles between two NRs changed, resulting in reversible modulation of the CD signals in the range of 75–225 mdeg.

Acid-base equilibrium and pH response of chiral assemblies can be used to adjust the chiroptical activity of NR dimers. Liu and co-workers[84] described a pH-responsive DNA triplex used to lock one NR of DNA origami assembled NR dimers. The triplex was decomposed to a single-stranded DNA and a DNA duplex with increased pH and recombined with decreased pH, thus generating lock and relaxed states for NR dimers. Just as in the previous example, during the transition of these two states the angles between two NRs changed, leading to the dynamic modulation of chiroptical activities.

Light was used to alter azobenzene-modified DNA lock to reversibly alter the structure of gold NR dimers assembled by DNA origami.[60] When the dimers were illuminated with UV light, the azobenzene was in the *trans* form, leading to the dehybridization state of DNA locks and the relaxed state of NR dimers. When visual light (400–700 nm) was used, the azobenzene was in the *cis* form, leading to the hybridization state of DNA locks and the locked state of NR dimers. During the transition of the lock and relaxed states of NR dimers, their angles were changed repeatedly, inducing the periodic adjustment to the CD signals.

In addition to the previously described environmental conditions, the reconfiguration of CNs can be performed *via* the interaction of chiral templates with functional molecules. CNs made by the DNA origami method with conformational changes mediated by DNA-toeholds was designed to fabricate helical assemblies with reversible reconfiguration (Figure 3b).[103] When the inter-arm angle of the template was changed *via* a toehold-mediated strand displacement reaction with different key strands and lock strands, the conformations of NR helices were converted between a tightly folded state and an extended state. Similarly, when the geometry of the template was altered by different block strands and release strands, the conformations of the NR helices were converted between left- and right-handed states.[104]

Mechanical modulation: Several pioneering works described that mechanical modulation can be used to achieve variation of chiroptical activity under mechanical operations, for example, stretching, bending, twisting, and compressing materials containing CNs. Our group[95] used a mechanical deformation to modulate achiral gold NPs to generate reversible plasmonic chiroptical activities *via* controlling the directions of the macroscale stretching to nanocomposites made by elastic substrates with layer-by-layer assembled gold NPs films (Figure 3e). The stretching changed the degree of chirality of the NP chains at the subnanometer scale that led to modulation of chiroptical responses under different strains. The modulated polarization of light was demonstrated for both the visible and near infrared parts of the spectrum with hundreds of modulation cycles [107]. Similarly, the strain of prefabricated CNs made from kirigami composites were used to modulate polarization rotation in the terahertz (THz) part of the spectrum (Figure 3d).[108] While it was fundamentally difficult to produce a polarization modulator for THz region with real-time reversible polarization rotation exceeding 45 degrees, plasmonic kirigami with chiral out-of-plane geometries made it possible. Modulations with cyclability over thousands of cycles facilitated practical implementation of THz circular dichroism (TCD) for the studies of various biomaterials.[108]

Similar with stretching CNs, bending and twisting can also make achiral composites chiral. Yin and co-workers[109] made a plasmonic film of well-aligned magnetic-plasmonic hybrid nanorods, which was twisted into left- and right-handed helices with reversed CD spectra from plasmonic CNs. Additionally, the compression decreased the distance between neighboring NPs and bent the nanochains to modulate chiroptical activity as observed by CD peaks, which was seen in the plasmonic film assembled by macroscopic stacking of achiral chain substrates.[19]

In addition to mechanical deformation in macroscale, mechanical modulation can be proceeded in nano/microscale. Fang and co-workers[79] used focused ion beam (FIB) to buckle the nano-kirigami film to fabricate 2D and 3D pinwheel arrays with different handedness, which generated programed CD signals and optical rotation.

Applications of Chiral Nanostructures

As numerous efforts have been made on the fabrication of inorganic CNs, the understanding of how to generate CNs and adjust their chiroptical activities have achieved much progress. CNs have gradually extended to all categories of nanomaterials, for example, metal, semiconductors, ceramic NPs, and carbon nanomaterials from gold clusters with weak CD[110] to highly optically active NP assemblies enabling multiple technological translations. A pathway to some emerging chirality-related applications have already been revealed, including low-noise biosensing,[111] biomimetic chiral catalysis,[36] polarization detectors,[112,113] and various implementations of chiral-induced spin selectivity (CISS) effect.[33,114,115]

Biosensing and biomedicine. Among these prospects, chirality-based biosensors have gathered the widest attention, as CNs are generally constituted by chiral biomolecule scaffolds, thus providing a good opportunity to develop biologically-related applications. During the last decade, chirality-based biosensors have achieved great progress. Various biosensors made of NPs have been designed by Xu and coworkers for the detection of heavy metal ions, biotoxins, antibiotics, RNAs, DNAs, enzymes, peptides, proteins, and other functional biomolecules, with limitations decreased to the attomolar level both *in vitro* and *in vivo* (Figure 4a).[35,116,117] The next phase of this work will be translation into the clinic and subsequent commercialization.

The left- and right-handed enantiomers of certain CNs will interact differently with biological nanostructures, for instance,

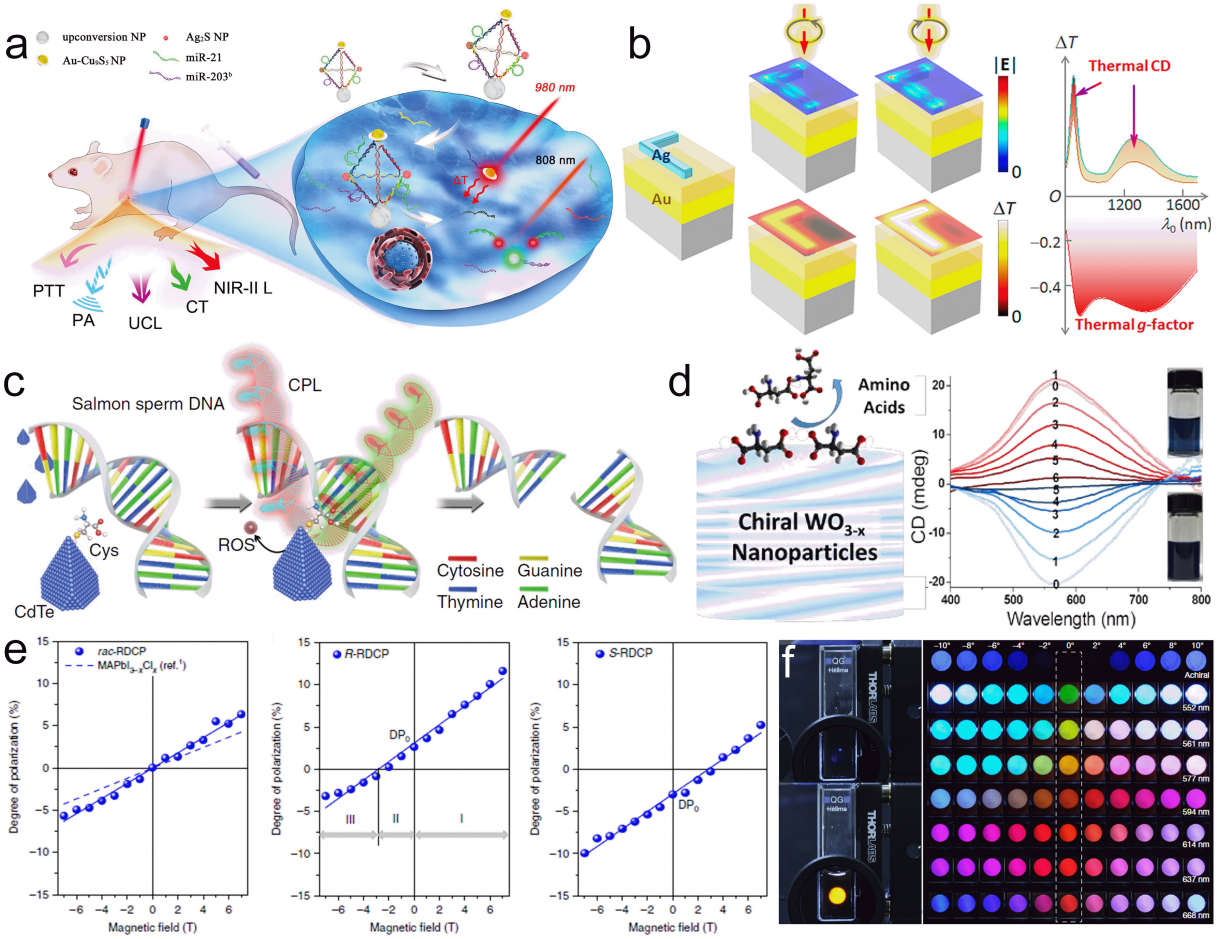

Figure 4. Advanced applications of CNs. (a) Nanopyramids assembled by Au–Cu_9S_5, upconversion and Ag_2S NPs with DNA molecules for the dual microRNA detection and bioimaging *in vivo*. Reproduced with permission from ref. [117]. Copyright 2017 John Wiley and Sons. (b) Photothermal circular dichroism system composed of chiral metamaterial absorbers with circularly polarized light beams, show the chiral photothermal effect under LCP and RCP. Reproduced with permission from ref. [131]. Copyright 2018 American Chemical Society. (c) Specific DNA cleavage by chiral CdTe NPs under circularly polarized irradiation. Reproduced with permission from ref. [118]. Copyright 2018 Springer Nature. (d) Catalysis of aspartic acid into dipeptide by chiral WO_{3-x}. Reproduced with permission from ref. [36]. Copyright 2018 American Chemical Society. (e) Degree of polarization of photoluminescence for reduced-dimensional chiral perovskites (RDCP) under different magnetic fields. Reproduced with permission from ref. [38]. Copyright 2018 Springer Nature. (f) Photon polarization and polarization-resolved colors for chiral helicoid NPs with high *g*-factors. Reproduced with permission from ref .[14]. Copyright 2018 Springer Nature.

endonuclease-like cleavage of DNA.[118] Among various CNs particular significance in this direction should be placed on chiral carbon nanodots and related nanostructures.[41,119,120] For example, Jelinek and coworkers[120] observed that enantiomeric carbon dots synthesized from *L*- and *D*-lysine, interacted very differently with amyloid beta-42 (Aβ42) peptide associated with Alzheimer's disease. In particular, carbon dots from *L*-lysine strongly altered the secondary structure and fibril morphologies of Aβ42, opening the realistic pathway to employ chiral nanocarbons as biomimetic therapeutics.

CNs with high *g*-factors have markedly different absorption coefficients for LCP and RCP. Consequently, the chiral surfaces can generate apparent differences in the electromagnetic fields and photoinduced temperatures (Figure 4b). Chiral photothermal effect disclosed by Orrit and co-workers in a recent work with planar chiral gold arrays[121] offer multiple venues for biomedical applications. The chiral photothermal effect with CNs may extend to photothermal therapy on cancers or other diseases. Beyond the laser frequency and wavelength, the polarization direction of circularly polarized light will provide a new modulation strategy and specific selectivity for photothermal therapy in clinical practices.

Chiral catalysis. Another promising prospect for CNs is to use chiral NPs for biomimetic chiral catalysis. Because CNs are comprised of both chiral molecules and inorganic NPs, it may be possible to simulate the biological catalysis function in nature. Compared to catalysts at the molecular scale, chiral NPs provide a curved nanoscale surface, which increases the retention time of reagents, leading to decreased energy barriers for chemical reactions. One good example is single ceramic

NPs of $WO_{3-x} \cdot H_2O$,[36] which showed catalytic activity for the formation of dipeptides when aspartic acid was used as the NP capping ligand (Figure 4d). Additionally, chiral NPs provide specific binding sites through the packing structure of capping ligands and generate reactive oxygen species for catalysis reactions under circularly polarized irradiation. In the research of Kuang, Kotov and co-workers,[118] cysteine-capped CdTe NPs specifically recognized the binding sites of GATATC sequences on double-stranded DNA chains. Under the illumination of circularly polarized light, CdTe NPs generate reactive oxygen species on NP surfaces, which were transferred to the binding site and cut the DNA strands (Figure 4c). Similarly, the catalysis process and mechanism has been applied to photocatalytic protein cleavages using chiral copper sulfide NPs.[122] Furthermore, chiral nanoparticles can provide chiral bias for the photo-oxidation and photo-reduction reactions that are particularly effective for semiconductor NPs. For example, ZnS NPs assembled into chiral supraparticles[82] provided strong chiral bias for the enantioselective oxidative phenol coupling to tyrosine dimerization.

Chiral photonics. Besides the established translational efforts with CNs discussed above, technological possibilities entered the conference and board rooms only recently. One technology in parallel with the emerging research trends discussed above, is the use of CNs for circular polarization modulation, which leads to the polarization-dependent color effect for the light transmitted through CNs. In the work of Nam and co-workers,[14] distinct green to red colors were observed when light was passed through two crossed polarizers between helicoid NPs with different resonance wavelengths (Figure 4f). More colors, in fact the whole color map, were achieved by altering the angles between the polarizers, adjusting the resonance wavelengths of chiral NPs, and mixing NPs in different wavelengths. These modulations provide possibilities to use CNs to adjust the colors for display, which are usually actualized by liquid crystals and organic light-emitting diodes. Particularly effective stratergy is the polarization modulation for THz region using kirigami-structured CNs,[108] enabling a new spectroscopic and imaging toolbox for biomaterials.

Another related emerging application is to use CNs to control photon polarization for emitted photons that is typically associated with luminescence but can also involve differentia scattering.[123] During the excitation process under LCP and RCP, CNs have different absorption rates of the spin-polarized photons. Similarly, in the emission process from the excited state to ground state, the excited electrons have different spin-polarized emission rates for the left- and right-handed spin-polarized emission, inducing different circular polarized luminescence. This circular polarized luminescence has been reported for NPs,[124] carbon dots,[125] metal clusters,[126] up-conversion NPs,[127] perovskites,[81,128] and transition metal dichalcogenides.[129] With the rapid development of CNs with circularly polarized luminescence, the external field-controlled emission becomes urgent due to the practical application needs in chiral light source as well as the related applications in sensing, imaging and lasers. In a recent work of Takenobu and co-workers,[129] they used an asymmetric strain to break the symmetry of tungsten disulfide monolayer to fabricate chiral light-emitting diode with electrically tunable ability, which paved a way for the fabrication of practical chiral light source. Additionally, magnetic fields have been found to be responsive to photon spin polarized luminescence according to effect of spin-orbit coupling and Zeeman splitting.[38,130] In the work of Sargent and co-workers,[38] perovskites exhibited 3% spin-polarized photoluminescence without a magnetic field. Once magnetic fields were applied, the Zeeman splitting adjusted to the valance and conduction bands of the chiral perovskites, which led to the linear modulation on the degree of spin polarization for photoluminescence with the magnetic field intensities (Figure 4e).

Conclusions and Outlook

The field of CNs has achieved significant progress and continues to grow. Considering the next decade, multiple fundamental and technological challenges still need to be addressed. One is the transition from laboratory to pilot-plant synthesis of CNs covering a broad range of materials while retaining high *g*-factors and other optical parameters. We also expect that CNs will be used in a variety of nanocomposites that are suitable for integration in wearable and other devices. Further, molecular mechanisms, theoretical models, and biological parallels of optical processes, chemical reactions and biological effects involving CNs will be elaborated based on multiscale hierarchical chirality concepts being developed, which is likely to require multidisciplinary cooperation from researchers in physics, chemistry, materials, and biochemistry. We also expect the spectrum of CNs to at least double in the next decade and address problems in catalysis, biology, medicine, biotechnology, nonlinear optics, photonics, and quantum effects.

Acknowledgments

This work was supported by the NSF project "Energy- and Cost-Efficient Manufacturing Employing Nanoparticles" NSF 1463474 and Vannevar Bush DoD Fellowship to N.A.K. titled "Engineered Chiral Ceramics" ONR N000141812876. NSF 1566460 "Nanospiked Particles for Photocatalysis", NSF 1538180 is also gratefully acknowledged.

References

[1] M. Lahav, L. Leiserowitz, *Phys. Scr.* **2015**, *90*, 118003.
[2] L. Addadi, Z. Berkovitch-Yellin, I. Weissbuch, J. Van Mil, L. J. W. Shimon, M. Lahav, L. Leiserowitz, *Angew. Chem. Int. Ed. Engl.* **1985**, *24*, 466.
[3] N. Lahav, D. White, S. Chang, *Science* **1978**, *201*, 67.

[4] I. Weissbuch, R. Popovitz-Biro, M. Lahav, L. Leiserowitz, Rehovot, *Acta Crystallogr. Sect. B* **1995**, *51*, 115.
[5] E. M. Landau, M. Levanon, L. Leiserowitz, M. Lahav, J. Sagiv, *Nature* **1985**, *318*, 353.
[6] H. Zepik, E. Shavit, M. Tang, T. R. Jensen, K. Kjaer, G. Bolbach, L. Leiserowitz, I. Weissbuch, M. Lahav, *Science* **2002**, *295*, 1266.
[7] A. Brack, *Handb. Clay Sci.* **2006**, *1*, 379.
[8] P. W. Lucas, J. H. Hough, J. Bailey, A. Chrysostomou, T. M. Gledhill, A. Mccall, *Origins Life Evol. Biospheres* **2005**, *35*, 29.
[9] D. G. Blackmond, *Proc. Natl. Acad. Sci. USA* **2004**, *101*, 5732.
[10] N. A. Kotov, *Europhys. Lett.* **2017**, *119*, 66008.
[11] W. Jiang, Z. Qu, P. Kumar, D. Vecchio, Y. Wang, Y. Ma, J. H. Bahng, K. Bernardino, W. R. Gomes, F. M. Colombari, A. Lozada-Blanco, M. Veksler, E. Marino, A. Simon, C. Murray, S. R. Muniz, A. F. de Moura, N. A. Kotov, *Science* **2020**, *368*, 642.
[12] S. Toxvaerd, *Int. J. Astrobiol.* **2005**, *4*, 43.
[13] J.-Y. Kim, J. Yeom, G. Zhao, H. Calcaterra, J. Munn, P. Zhang, N. Kotov, *J. Am. Chem. Soc.* **2019**, *141*, 11739.
[14] H. E. Lee, H. Y. Ahn, J. Mun, Y. Y. Lee, M. Kim, N. H. Cho, K. Chang, W. S. Kim, J. Rho, K. T. Nam, *Nature* **2018**, *556*, 360.
[15] J. Lu, Y. Xue, K. Bernardino, N. N. Zhang, W. R. Gomes, N. S. Ramesar, S. Liu, Z. Hu, T. Sun, A. F. de Moura, N. A. Kotov, K. Liu, *Science* **2021**, *371*, 1368.
[16] A. S. Baimuratov, I. D. Rukhlenko, R. E. Noskov, P. Ginzburg, Y. K. Gun'ko, A. V. Baranov, A. V. Fedorov, *Sci. Rep.* **2015**, *5*, 14712.
[17] A. Y. Zhu, W. T. Chen, A. Zaidi, Y.-W. Huang, M. Khorasaninejad, V. Sanjeev, C.-W. Qiu, F. Capasso, *Light-Sci. Appl.* **2018**, *7*, 17158.
[18] J. Chi, H. Liu, Z. Wang, N. Huang, *Opt. Express* **2020**, *28*, 4529.
[19] P. T. Probst, M. Mayer, V. Gupta, A. M. Steiner, Z. Zhou, G. K. Auernhammer, T. A. F. König, A. Fery, *Nat. Mater.* **2021**, *20*, 1024.
[20] J. T. Collins, C. Kuppe, D. C. Hooper, C. Sibilia, M. Centini, V. K. Valev, *Adv. Opt. Mater.* **2017**, *5*, 1700182.
[21] T. G. Schaaff, R. L. Whetten, *J. Phys. Chem. B* **2000**, *104*, 2630.
[22] M. P. Moloney, Y. K. Gun'ko, J. M. Kelly, *Chem. Commun.* **2007**, *38*, 3900.
[23] W. Chen, A. Bian, A. Agarwal, L. Liu, H. Shen, L. Wang, C. Xu, N. A. Kotov, *Nano Lett.* **2009**, *9*, 2153.
[24] A. Guerrero-Martínez, B. Auguié, J. L. Alonso-Gómez, Z. Džolić, S. Gómez-Graña, M. Žinić, M. M. Cid, L. M. Liz-Marzán, *Angew. Chem. Int. Ed.* **2011**, *50*, 5499.
[25] J. Zhu, F. Wu, Z. Han, Y. Shang, F. Liu, H. Yu, L. Yu, N. Li, B. Ding, *Nano Lett.* **2021**, *21*, 3573.
[26] G. Shemer, O. Krichevski, G. Markovich, T. Molotsky, I. Lubitz, A. B. Kotlyar, *J. Am. Chem. Soc.* **2006**, *128*, 11006.
[27] J. K. Gansel, M. Thiel, M. S. Rill, M. Decker, K. Bade, V. Saile, G. von Freymann, S. Linden, M. Wegener, *Science* **2009**, *325*, 1513.
[28] A. Guerrero-Martínez, M. Grzelczak, L. M. Liz-Marzán, *ACS Nano* **2012**, *6*, 3655.
[29] W. Ma, L. Xu, A. F. de Moura, X. Wu, H. Kuang, C. Xu, N. A. Kotov, *Chem. Rev.* **2017**, *117*, 8041.
[30] V. Anastasia, N. A. Kotov, *CCS Chem.* **2020**, *2*, 583.
[31] J. E. Govan, E. Jan, A. Querejeta, N. A. Kotov, Y. K. Gun'ko, *Chem. Commun.* **2010**, *46*, 6072.
[32] J. Butet, P. F. Brevet, O. J. F. Martin, *ACS Nano* **2015**, *9*, 10545.
[33] H. Lu, J. Wang, C. Xiao, X. Pan, X. Chen, R. Brunecky, J. J. Berry, K. Zhu, M. C. Beard, Z. V. Vardeny, *Sci. Adv.* **2019**, *5*, eaay0571.
[34] G. Long, R. Sabatini, M. I. Saidaminov, G. Lakhwani, A. Rasmita, X. Liu, E. H. Sargent, W. Gao, *Nat. Rev. Mater.* **2020**, *5*, 423.
[35] X. Wu, C. Hao, J. Kumar, H. Kuang, N. A. Kotov, L. M. Liz-Marzán, C. Xu, *Chem. Soc. Rev.* **2018**, *47*, 4677.
[36] S. Jiang, M. Chekini, Z. B. Qu, Y. Wang, A. Yeltik, Y. Liu, A. Kotlyar, T. Zhang, B. Li, H. V. Demir, N. A. Kotov, *J. Am. Chem. Soc.* **2017**, *139*, 13701.
[37] D. Schamel, M. Pfeifer, J. G. Gibbs, B. Miksch, A. G. Mark, P. Fischer, *J. Am. Chem. Soc.* **2013**, *135*, 12353.
[38] G. Long, C. Jiang, R. Sabatini, Z. Yang, M. Wei, L. N. Quan, Q. Liang, A. Rasmita, M. Askerka, G. Walters, X. Gong, J. Xing, X. Wen, R. Quintero-Bermudez, H. Yuan, G. Xing, X. R. Wang, D. Song, O. Voznyy, M. Zhang, S. Hoogland, W. Gao, Q. Xiong, E. H. Sargent, *Nat. Photonics* **2018**, *12*, 528.
[39] S. D. Elliott, M. P. Moloney, Y. K. Gun'ko, *Nano Lett.* **2008**, *8*, 2452.
[40] Y. Zhou, M. Yang, K. Sun, Z. Tang, N. A. Kotov, *J. Am. Chem. Soc.* **2010**, *132*, 6006.
[41] N. Suzuki, Y. Wang, P. Elvati, Z.-B. Qu, K. Kim, S. Jiang, E. Baumeister, J. Lee, B. Yeom, J. H. Bahng, J. Lee, A. Violi, N. A. Kotov, *ACS Nano* **2016**, *10*, 1744.
[42] A. O. Govorov, Z. Fan, P. Hernandez, J. M. Slocik, R. R. Naik, *Nano Lett.* **2010**, *10*, 1374.
[43] B. M. Maoz, Y. Chaikin, A. B. Tesler, O. Bar Elli, Z. Fan, A. O. Govorov, G. Markovich, *Nano Lett.* **2013**, *13*, 1203.
[44] J. Yeom, U. S. Santos, M. Chekini, M. Cha, A. F. De Moura, N. A. Kotov, *Science* **2018**, *359*, 309.
[45] V. A. Gérard, Y. K. Gun'Ko, E. Defrancq, A. O. Govorov, *Chem. Commun.* **2011**, *47*, 7383.
[46] A. Ben-Moshe, A. Teitelboim, D. Oron, G. Markovich, *Nano Lett.* **2016**, *16*, 7467.
[47] J. M. Slocik, A. O. Govorov, R. R. Naik, *Nano Lett.* **2011**, *11*, 701.
[48] U. Hananel, A. Ben-Moshe, D. Tal, G. Markovich, *Adv. Mater.* **2019**, *32*, 1905594.
[49] F. D. Saeva, G. R. Olin, J. Y. C. Chu, *Mol. Cryst. Liq. Cryst.* **1977**, *41*, 5.
[50] A. Ben-Moshe, S. G. Wolf, M. B. Sadan, L. Houben, Z. Fan, A. O. Govorov, G. Markovich, *Nat. Commun.* **2014**, *5*, 4302.
[51] U. Hananel, A. Ben-Moshe, H. Diamant, G. Markovich, *Proc. Natl. Acad. Sci. USA* **2019**, *116*, 11159.
[52] P. P. Wang, S. J. Yu, A. O. Govorov, M. Ouyang, *Nat. Commun.* **2017**, *8*, 14312.
[53] A. S. Baimuratov, I. D. Rukhlenko, Y. K. Gun'ko, A. V. Baranov, A. V. Fedorov, *Nano Lett.* **2015**, *15*, 1710.
[54] F. Purcell-Milton, R. McKenna, L. J. Brennan, C. P. Cullen, L. Guillemeney, N. V. Tepliakov, A. S. Baimuratov, I. D. Rukhlenko, T. S. Perova, G. S. Duesberg, A. V. Baranov, A. V. Fedorov, Y. K. Gun'ko, *ACS Nano* **2018**, *12*, 954.
[55] A. Ben-Moshe, A. da Silva, A. Müller, A. Abu-Odeh, P. Harrison, J. Waelder, F. Niroui, C. Ophus, A. M. Minor, M. Asta, W. Theis, P. Ercius, A. P. Alivisatos, *Science* **2021**, *372*, 729.
[56] I. L. Garzón, J. A. Reyes-Nava, J. I. Rodríguez-Hernández, I. Sigal, M. R. Beltrán, K. Michaelian, *Phys. Rev. B* **2002**, *66*, 73403.
[57] S. Knoppe, O. A. Wong, S. Malola, H. Häkkinen, T. Bürgi, T. Verbiest, C. J. Ackerson, *J. Am. Chem. Soc.* **2014**, *136*, 4129.
[58] J. Ahn, E. Lee, J. Tan, W. Yang, B. Kim, J. Moon, *Mater. Horiz.* **2017**, *4*, 851.
[59] A. Kuzyk, R. Schreiber, Z. Fan, G. Pardatscher, E.-M. Roller, A. Högele, F. C. Simmel, A. O. Govorov, T. Liedl, *Nature* **2012**, *483*, 311.

[60] A. Kuzyk, Y. Yang, X. Duan, S. Stoll, A. O. Govorov, H. Sugiyama, M. Endo, N. Liu, *Nat. Commun.* **2016**, *7*, 10591.
[61] E. Prodan, C. Radloff, N. J. Halas, P. Nordlander, *Science* **2003**, *302*, 419.
[62] W. Yan, L. Xu, C. Xu, W. Ma, H. Kuang, L. Wang, N. A. Kotov, *J. Am. Chem. Soc.* **2012**, *134*, 15114.
[63] T. Hu, B. P. Isaacoff, J. H. Bahng, C. Hao, Y. Zhou, J. Zhu, X. Li, Z. Wang, S. Liu, C. Xu, J. S. Biteen, N. A. Kotov, *Nano Lett.* **2014**, *14*, 6799.
[64] Y. Guo, G. Zhu, Y. Fang, *J. Appl. Phys.* **2021**, *129*, 43104.
[65] N. T. Fofang, N. K. Grady, Z. Fan, A. O. Govorov, N. J. Halas, *Nano Lett.* **2011**, *11*, 1556.
[66] J. Sun, Y. Li, H. Hu, W. Chen, D. Zheng, S. Zhang, H. Xu, *Nanoscale* **2021**, *13*, 4408.
[67] X. Lan, X. Lu, C. Shen, Y. Ke, W. Ni, Q. Wang, *J. Am. Chem. Soc.* **2015**, *137*, 457.
[68] J. Lu, Y. X. Chang, N. N. Zhang, Y. Wei, A. J. Li, J. Tai, Y. Xue, Z. Y. Wang, Y. Yang, L. Zhao, Z. Y. Lu, K. Liu, *ACS Nano* **2017**, *11*, 3463.
[69] S. Mokashi-Punekar, A. D. Merg, N. L. Rosi, *J. Am. Chem. Soc.* **2017**, *139*, 15043.
[70] A. Querejeta-Fernández, G. Chauve, M. Methot, J. Bouchard, E. Kumacheva, *J. Am. Chem. Soc.* **2014**, *136*, 4788.
[71] M. Bagiński, M. Tupikowska, G. González-Rubio, M. Wójcik, W. Lewandowski, *Adv. Mater.* **2020**, *32*, 1904581.
[72] G. Cheng, D. Xu, Z. Lu, K. Liu, *ACS Nano* **2019**, *13*, 1479.
[73] J. Yan, W. Feng, J.-Y. Kim, J. Lu, P. Kumar, Z. Mu, X. Wu, X. Mao, N. A. Kotov, *Chem. Mater.* **2020**, *32*, 476.
[74] F. Serafin, J. Lu, N. Kotov, K. Sun, X. Mao, *Nat. Commun.* **2021**, *12*, 4925.
[75] M. Esposito, V. Tasco, F. Todisco, M. Cuscunà, A. Benedetti, D. Sanvitto, A. Passaseo, *Nat. Commun.* **2015**, *6*, 6484.
[76] A. G. Mark, J. G. Gibbs, T.-C. Lee, P. Fischer, *Nat. Mater.* **2013**, *12*, 802.
[77] B. Frank, X. Yin, M. Schäferling, J. Zhao, S. M. Hein, P. V. Braun, H. Giessen, *ACS Nano* **2013**, *7*, 6321.
[78] L. Jing, Z. Wang, B. Zheng, H. Wang, Y. Yang, L. Shen, W. Yin, E. Li, H. Chen, *NPG Asia Materials* **2018**, *10*, 888.
[79] Z. Liu, H. Du, J. Li, L. Lu, Z.-Y. Li, N. X. Fang, *Sci. Adv.* **2018**, *4*, eaat4436.
[80] T. Molotsky, T. Tamarin, A. Ben Moshe, G. Markovich, A. B. Kotlyar, *J. Phys. Chem. C* **2010**, *114*, 15951.
[81] J.-X. Gao, W.-Y. Zhang, Z.-G. Wu, Y.-X. Zheng, D.-W. Fu, *J. Am. Chem. Soc.* **2020**, *142*, 4756.
[82] S. Li, J. Liu, N. S. Ramesar, H. Heinz, L. Xu, C. Xu, N. A. Kotov, *Nat. Commun.* **2019**, *10*, 4826.
[83] W. Ma, H. Kuang, L. Wang, L. Xu, W.-S. Chang, H. Zhang, M. Sun, Y. Zhu, Y. Zhao, L. Liu, C. Xu, S. Link, N. A. Kotov, *Sci. Rep.* **2013**, *3*, 1934.
[84] A. Kuzyk, M. J. Urban, A. Idili, F. Ricci, N. Liu, *Sci. Adv.* **2017**, *3*, e1602803.
[85] Z. Wang, L. Jing, K. Yao, Y. Yang, B. Zheng, C. M. Soukoulis, H. Chen, Y. Liu, *Adv. Mater.* **2017**, *29*, 1700412.
[86] W. Feng, J.-Y. Kim, X. Wang, H. A. Calcaterra, Z. Qu, L. Meshi, N. A. Kotov, *Sci. Adv.* **2017**, *3*, e1601159.
[87] R. Del Villar-Guerra, R. D. Gray, J. B. Chaires, *Curr. Protoc. Nucleic Acid Chem.* **2017**, *68*, 17.8. 1.
[88] B. R. Baker, R. L. Garrell, *Faraday Discuss.* **2004**, *126*, 209.
[89] J. K. Choi, B. E. Haynie, U. Tohgha, L. Pap, K. W. Elliott, B. M. Leonard, S. V. Dzyuba, K. Varga, J. Kubelka, M. Balaz, *ACS Nano* **2016**, *10*, 3809.
[90] B. M. Maoz, R. Van Der Weegen, Z. Fan, A. O. Govorov, G. Ellestad, N. Berova, E. W. Meijer, G. Markovich, *J. Am. Chem. Soc.* **2012**, *134*, 17807.
[91] M. C. Di Gregorio, A. Ben Moshe, E. Tirosh, L. Galantini, G. Markovich, *J. Phys. Chem. C* **2015**, *119*, 17111.
[92] G. González-Rubio, J. Mosquera, V. Kumar, A. Pedrazo-Tardajos, P. Llombart, D. M. Solís, I. Lobato, E. G. Noya, A. Guerrero-Martínez, J. M. Taboada, F. Obelleiro, L. G. MacDowell, S. Bals, L. M. Liz-Marzán, *Science* **2020**, *368*, 1472.
[93] J. Lv, K. Hou, D. Ding, D. Wang, B. Han, X. Gao, M. Zhao, L. Shi, J. Guo, Y. Zheng, X. Zhang, C. Lu, L. Huang, W. Huang, Z. Tang, *Angew. Chem. Int. Ed.* **2017**, *56*, 5055.
[94] K. Ding, J. Ai, Q. Deng, B. Huang, C. Zhou, T. Duan, Y. Duan, L. Han, J. Jiang, S. Che, *Angew. Chem.* **2021**, *133*, 19172.
[95] Y. Kim, B. Yeom, O. Arteaga, S. J. Yoo, S.-G. Lee, J.-G. Kim, N. A. Kotov, *Nat. Mater.* **2016**, *15*, 461.
[96] M. Esposito, V. Tasco, M. Cuscunà, F. Todisco, A. Benedetti, I. Tarantini, M. De Giorgi, D. Sanvitto, A. Passaseo, *ACS Photonics* **2015**, *2*, 105.
[97] S. Zu, Y. Bao, Z. Fang, *Nanoscale* **2016**, *8*, 3900.
[98] Y. Yang, J. Liang, F. Pan, Z. Wang, J. Zhang, K. Amin, J. Fang, W. Zou, Y. Chen, X. Shi, Z. Wei, *Nat. Commun.* **2018**, *9*, 3808.
[99] L. Shi, L. Zhu, J. Guo, L. Zhang, Y. Shi, Y. Zhang, K. Hou, Y. Zheng, Y. Zhu, J. Lv, S. Liu, Z. Tang, *Angew. Chem. Int. Ed.* **2017**, *56*, 15397.
[100] J. Yan, S. Hou, Y. Ji, X. Wu, *Nanoscale* **2016**, *8*, 10030.
[101] M. Hentschel, M. Schäferling, T. Weiss, N. Liu, H. Giessen, *Nano Lett.* **2012**, *12*, 2542.
[102] C. Zhou, L. Xin, X. Duan, M. J. Urban, N. Liu, *Nano Lett.* **2018**, *18*, 7395.
[103] X. Lan, T. Liu, Z. Wang, A. O. Govorov, H. Yan, Y. Liu, *J. Am. Chem. Soc.* **2018**, *140*, 11763.
[104] C. Zhou, X. Duan, N. Liu, *Nat. Commun.* **2015**, *6*, 8102.
[105] M. Sun, L. Xu, J. H. Banhg, H. Kuang, S. Alben, N. A. Kotov, C. Xu, *Nat. Commun.* **2017**, *8*, 1847.
[106] Z. Li, Z. Zhu, W. Liu, Y. Zhou, B. Han, Y. Gao, Z. Tang, *J. Am. Chem. Soc.* **2012**, *134*, 3322.
[107] L. Xu, T. C. Shyu, N. A. Kotov, *ACS Nano* **2017**, *11*, 7587.
[108] W. Choi, G. Cheng, Z. Huang, S. Zhang, T. Norris, N. A. Kotov, *Nat. Mater.* **2019**, *18*, 820.
[109] Z. Li, J. Jin, F. Yang, N. Song, Y. Yin, *Nat. Commun.* **2020**, *11*, 2883.
[110] S. Knoppe, T. Bürgi, *Acc. Chem. Res.* **2014**, *47*, 1318.
[111] Y. Zhao, L. Xu, W. Ma, L. Wang, H. Kuang, C. Xu, N. A. Kotov, *Nano Lett.* **2014**, *14*, 3908.
[112] J. Hao, H. Lu, L. Mao, X. Chen, M. C. Beard, J. L. Blackburn, *ACS Nano* **2021**, *15*, 7608.
[113] X. Ma, M. Pu, X. Li, Y. Guo, P. Gao, X. Luo, *Nanomaterials* **2017**, *7*, 116.
[114] R. Naaman, D. H. Waldeck, *Annu. Rev. Phys. Chem.* **2015**, *66*, 263.
[115] R. Naaman, Y. Paltiel, D. H. Waldeck, *Nat. Rev. Chem.* **2019**, *3*, 250.
[116] W. Ma, L. Xu, L. Wang, C. Xu, H. Kuang, *Adv. Funct. Mater.* **2019**, *29*, 1805512.
[117] S. Li, L. Xu, M. Sun, X. Wu, L. Liu, H. Kuang, C. Xu, *Adv. Mater.* **2017**, *29*, 1606086.
[118] M. Sun, L. Xu, A. Qu, P. Zhao, T. Hao, W. Ma, C. Hao, X. Wen, F. M. Colombari, A. F. de Moura, N. A. Kotov, C. Xu, H. Kuang, *Nat. Chem.* **2018**, *10*, 821.
[119] S. K. Bhunia, A. R. Maity, S. Nandi, D. Stepensky, R. Jelinek, *ChemBioChem* **2016**, *17*, 614.
[120] E. Arad, S. K. Bhunia, J. Jopp, S. Kolusheva, H. Rapaport, R. Jelinek, *Adv. Ther.* **2018**, *1*, 1800006.
[121] P. Spaeth, S. Adhikari, L. Le, T. Jollans, S. Pud, W. Albrecht, T. Bauer, M. Caldarola, L. Kuipers, M. Orrit, *Nano Lett.* **2019**, *19*, 8934.

[122] C. Hao, R. Gao, Y. Li, L. Xu, M. Sun, C. Xu, H. Kuang, *Angew. Chem.* **2019**, *131*, 7449.
[123] L.-Y. Wang, K. W. Smith, S. Dominguez-Medina, N. Moody, J. M. Olson, H. Zhang, W.-S. Chang, N. A. Kotov, S. Link, *ACS Photonics* **2015**, *2*, 1602.
[124] J. Cheng, J. Hao, H. Liu, J. Li, J. Li, X. Zhu, X. Lin, K. Wang, T. He, *ACS Nano* **2018**, *12*, 5341.
[125] Y. Ru, L. Sui, H. Song, X. Liu, Z. Tang, S.-Q. Zang, B. Yang, S. Lu, *Angew. Chem. Int. Ed.* **2021**, *60*, 14091.
[126] J. Kumar, T. Kawai, T. Nakashima, *Chem. Commun.* **2017**, *53*, 1269.
[127] X. Jin, Y. Sang, Y. Shi, Y. Li, X. Zhu, P. Duan, M. Liu, *ACS Nano* **2019**, *13*, 2804.
[128] Y. Shi, P. Duan, S. Huo, Y. Li, M. Liu, *Adv. Mater.* **2018**, *30*, 1705011.
[129] J. Pu, W. Zhang, H. Matsuoka, Y. Kobayashi, Y. Takaguchi, Y. Miyata, K. Matsuda, Y. Miyauchi, T. Takenobu, *Adv. Mater.* **2021**, *33*, 2100601.
[130] C. Zhang, D. Sun, C.-X. Sheng, Y. X. Zhai, K. Mielczarek, A. Zakhidov, Z. V. Vardeny, *Nat. Phys.* **2015**, *11*, 427.
[131] X.-T. Kong, L. Khosravi Khorashad, Z. Wang, A. O. Govorov, *Nano Lett.* **2018**, *18*, 2001.

Manuscript received: July 16, 2021
Revised manuscript received: September 3, 2021
Version of record online: November 5, 2021